Polyhedron 269 (2025) 117395

Contents lists available at ScienceDirect

Polyhedron

journal homepage: www.elsevier.com/locate/poly

The synthesis, structure and solution and gas phase properties of complexes of scandium and lanthanide triflates with the phosphine oxide ligands $PhP(O)(C_2H_4P(O)Ph_2)_2$ and $P(O)(C_2H_4P(O)Ph_2)_3$ ☆

Simon J. Coles [a], Ann P. Hunter [b], Sarah J. Fieldhouse [c], Anthony M.J. Lees [c], Laura J. McCormick McPherson [a], Andrew W.G. Platt [c,*]

[a] UK National Crystallography Service, Department of Chemistry, University of Southampton, Highfield Campus, Southampton SO17 1BJ, UK
[b] National Mass Spectrometry Service Facility, Faculty of Medicine, Health & Life Science, Swansea University, Swansea SA2 8PP, UK
[c] School of Health, Education and Sciences, University of Staffordshire, Leek Road, Stoke-on-Trent ST4 2DF, UK

ARTICLE INFO

Keywords:
Lanthanide triflates
Structure
Polyphosphine oxide
NMR spectroscopy
Electrospray mass spectrometrey

ABSTRACT

The synthesis and structures of complexes of $PhP(O)(C_2H_4P(O)Ph_2)_2$, L^1, and $P(O)(C_2H_4P(O)Ph_2)_3$, L^2, respectively, with scandium and lanthanide triflates are described. Single crystal x-ray structures of complexes of the octahedral $[Sc(L^1)_3](OTf)_3$, dodecahedral $[Nd(OTf)(H_2O)(L^1)_2](OTf)_2$ and $[Ln(OTf)(H_2O)(L^2)_2](OTf)_2$ (Ln = La, Gd), and the dimeric $[\{Er(OTf)_2(H_2O)(\mu\text{–}L^2)\}_2](OTf)_2$ and $[\{Er(OTf)_2(EtOH)(\mu\text{–}L^2)\}_2](OTf)_2$, which have distorted pentagonal bipyramidal geometry around Er, have been determined. The solution properties of the complexes have been investigated by ^{19}F and ^{31}P NMR spectroscopy which show that the complexes of L^1 are fluxional with exchange of inequivalent coordinated Ph_2PO groups in solution. Complexes of L^2 show the same process and exchange between coordinated and pendant arms of the ligand. The stability in the gas phase has been investigated by electrospray mass spectrometry (ESMS) and tandem ESMS where, in addition to loss of triflate, L^1 and L^2, loss of diphenylphosphine oxide and $Ph_2P(O)C_2H_4OSO_2CF_3$ are shown to be significant decomposition pathways for complexes of both ligands. A brief study of the catalytic properties of a range of complexes shows that the alkenylation of 1,4-dimethoxybenzene with phenylacetylene in nitromethane does not occur at 80 °C for complexes of L^1 or L^2.

1. Introduction

Complexes between lanthanide ions and phosphine oxides of higher denticity than 2 are relatively scarce [1]. Coordination of tridentate ligands $CH(CH_2P(O)Ar_2)_3$ (Ar = Ph, 4-MeC_6H_4, 2-MeC_6H_4, 2,5-$Me_2C_6H_3$) with yttrium nitrate gives insoluble complexes which have a distorted tricapped trigonal prismatic structures [2] whilst the related $[Ln(NO_3)_3(MeC(CH_2P(O)Ph_2)_3)]$ (Ln = La, Pr) have polymeric structures with the ligand acting in chelating and bridging modes [3]. Lanthanide complexes with linear polyphosphine oxides $Ph_2P(O)(CH_2POPh)_nP(O)Ph_2$ (n = 1, 2), **1** and **2** respectively in Fig. 1, and their solvent extraction properties in nitrate and chloride solutions have been reported [4]. More recently the tridentate ligand (**3**) has been found to form a moncapped square antiprismatic complex with Eu hexafluoracetylacetonate [5], and the tetraphosphine oxide (**4**) forms the mononuclear $[Ce(NO_3)_3(\mathbf{4})]$ with all 4 PO groups coordinating to the Ce ion, whilst dimeric complexes $[\{Ln(hfa)_3\}_2(\mathbf{4})]$ (where Ln = Eu, Tb and hfa = hexafluoroacetylacetonate) have been characterised. The structure around each lanthanide ion is a capped square antiprism with (**4**) acting essentially as two bidentate ligands [6]. The rigid ligand structure of 1,2,4,5-$(Ph_2PO)_4C_6H_2$ (**5**) imposes a binuclear structure on its lanthanide nitrate complexes $[\{Ln(NO_3)_3\}_2(5)]$ (Ln = Eu, Tb)[7].

The trifluoromethane sulfonate, or triflate, ion is weakly coordinating to lanthanide ions, and as a result, lanthanide [8] and in particular scandium [9] triflates have been widely used as catalysts for a variety of organic transformations. The low affinity of triflate ions for Ln^{3+} has also been exploited in exploring catalytic properties of scandium and lanthanide complexes with polydentate nitrogen [10,11] and polyether ligands [12]. These act as catalysts for enantioselective Diels-Alder reactions [10], polymerisation [11], the allylation of aldehydes

☆ This article is part of a special issue entitled: 'f-element chemistry' published in Polyhedron.

* Corresponding author.
E-mail address: a.platt@staffs.ac.uk (A.W.G. Platt).

https://doi.org/10.1016/j.poly.2025.117395
Received 16 October 2024; Accepted 7 January 2025
Available online 16 January 2025

and Diels-Alder additions to cyclopentadiene [12]. We have investigated the formation, solid state structures, solution and gas phase properties of scandium and lanthanide triflate complexes of the multidentate $PhP(O)(CH_2CH_2P(O)Ph_2)_2$, L^1, and $P(O)(CH_2CH_2P(O)Ph_2)_3$, L^2 shown in Fig. 2, below, and briefly examined the catalytic alkenylation of 1,4-dimethoxy benzene with phenylacetylene.

We chose to study a range of metals with varying ionic radii and examine the effect of this on the coordination properties and structures of the resulting complexes. The choice of triflate as counterion was made on the basis that this is less likely to compete for coordination sites with the phosphine oxide and substrates in any catalytic process.

2. Results and discussion

The ligands were prepared by oxidation of the corresponding phosphine with H_2O_2 in acetone, and complexes formed by reaction of the ligands with scandium and lanthanide triflates in hot methanol or ethanol. This is summarised in Scheme 1. In many cases, particularly for complexes of L^2, crystals suitable for single crystal X-ray work formed spontaneously on cooling the reaction solutions and were isolated as air and moisture stable solids. Elemental analysis indicated that the bulk material had a composition with a 3:2 metal:ligand ratio and was thus different from the crystals isolated for the La and Gd complexes. In the case of erbium, a dimeric complex, $[\{Er(OTf)_2(H_2O)(\mu\text{–}L^2)\}_2](OTf)_2$, was obtained which on recrystallisation from ethanol gave $[\{Er(OTf)_2(EtOH)(\mu\text{–}L^2)\}_2](OTf)_2$. Complexes of L^1 were more difficult to obtain as single crystals. The scandium complex formed spontaneously and the neodymium complex could be obtained in a form suitable for single crystal x-ray diffraction on crystallisation from CH_2Cl_2 as $[Nd(OTf)(H_2O)(L^1)_2](OTf)_2{\cdot}3CH_2Cl_2$, whilst complexes for the heavier lanthanides gave elemental analysis consistent with 3:1 complexes $[Ln(OTf)_3(L^1)_3]$. This is despite the reactions being carried out with approximately 1:1 ratios of ligand to metal. We have previously encountered a similar situation in the formation of complexes of trinaphthylphosphine oxide, where 1:4 complexes only were isolated despite reactions being carried out with an excess of metal present [13]. We have been unable to obtain crystals of these materials suitable for single crystal x-ray diffraction studies. In the following discussion the inequivalent phosphorus atoms within the ligands are designated a and b as indicated by $PhP_a(O)(C_2H_4P_b(O)Ph_2)_2$ and $P_a(O)(C_2H_4P_b(O)Ph_2)_3$.

2.1. Solid state structures

Details of the data collection and refinement for all the complexes are given in the supplementary information and deposited cifs. The geometries around the metal ions were determined by continuous shape measures [14,15] which gives the sum of squares (S) of deviations of the coordinated atoms from their positions in idealised polyhedra. Values of S below 3 represent small distortions from the optimum geometry with higher values being indicative of more significant deviations. The principal distances and angles for the complexes are given in Table 1 with more extensive listings in the supplementary information. Many of the complexes showed significant disorder.

Hydrogen bonding is a common feature of the structures where the coordinated triflate ions and water/ethanol molecules occupy adjacent sites on the metal and leads to the formation of almost planar –Ln—O—H—O—S—O 6-membered rings. The average the O…O distance of 2.83 Å is significantly shorter than the sum of the Van der Waals radii for oxygen of 3.04 Å [16] indicating strong hydrogen bonding. In addition, there is often H-bonding between coordinated water/ethanol and ionic triflate with similar O…O and O…H distances observed.

2.2. Complexes of $PhP(O)(C_2H_4P(O)Ph_2)_2$, (L^1)

The structure of the octahedral Sc complex $[Sc(L^1)_2](OTf)_3$ (S = 0.23) is shown in Fig. 3. Selected bond distances and angles are given in Table 1 and a more comprehensive listing in the supplementary information. The geometry around the scandium ion is only slightly distorted from regular octahedral with average *cis*-O-Sc-O angles of 89.99° and the *trans*-O-Sc-O 174.77°. Each L^1 occupies a facial position around the

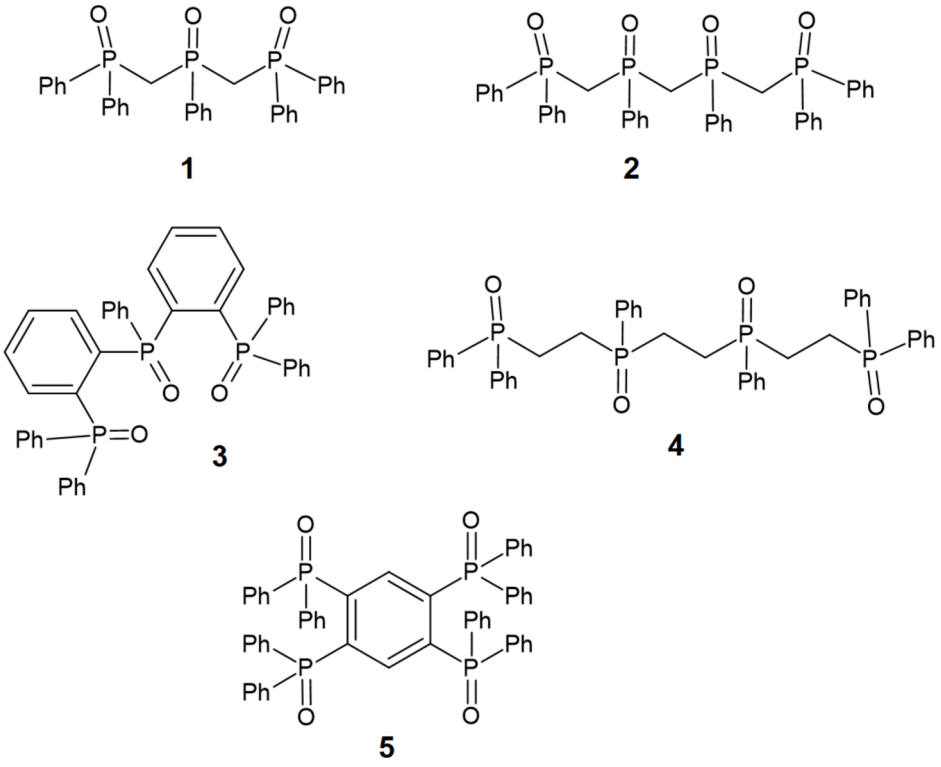

Fig. 1. Literature ligand structures.

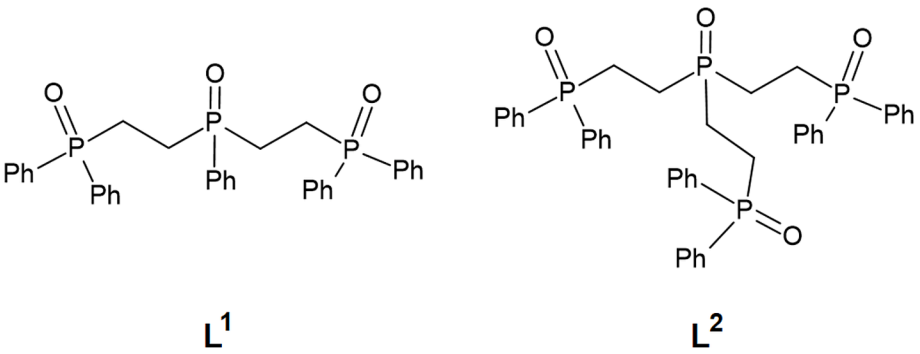

Fig. 2. Multidentate ligands used in this study.

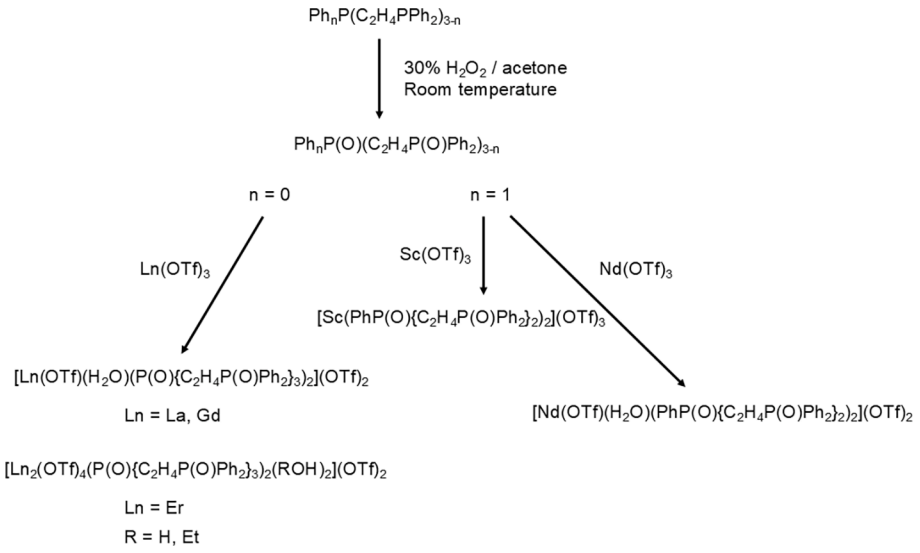

Scheme 1. Synthetic procedure for the ligands and structurally characterised complexes.

metal with the P_aO *trans* to a P_bO from the other ligand. The other P_bO groups are *trans* to each other, and thus the two P_b atoms are inequivalent. The angles around P_a range between 97.5° to 115.8° with an average of 108.1° which implies that the ligand structure is relatively unstrained when coordinated in a κ^3 manner.

The bond distances are very similar to those found in the closely related octahedral $[Sc(Ph_2P(O)CH_2P(O)Ph_2)_3]^{3+}$ which has an average Sc-O distance marginally longer at 2.091 Å and O-Sc-O bond angles little distorted from the expected 90° and 180° [17].

The Nd complex crystallised with two molecules in the unit cell. The geometry around each Nd ion is dodecahedral (S = 0.52 and 0.49). Fig. 4 shows one of the ions, the other is geometrically identical. In an ideal dodecahedron there are two sets of 4 coordinating atoms, designated x and y. The x set has four closest neighbours and here comprises two pairs; O1T, O1W from the triflate and water and O1, O4 from the P_aO groups of the two ligands. The y set is made up from the four P_bO groups and these have five close neighbours. The angle around P_a averages close to the ideal tetrahedral angle at 110.04 (3.8) ° which implies, again, that coordination in a tridentate fashion causes little or no strain within the L^1 structure.

Attempts to model disordered solvent were unsuccessful, and a solvent mask has been applied. This found the presence of 1.8 MeOH and 1.9 H_2O per $[Sc(L^1)_2]^{3+}$, and 3 CH_2Cl_2 molecules for every two $[Nd(OTf)(H_2O)(L^1)_2]^{2+}$ cations.

2.3. Complexes of $P(O)(C_2H_4P(O)Ph_2)_3$ (L^2)

The complexes of L^2 show variation with the size of the lanthanide ion. For the lighter metals the structures are based on a dication, $[Ln(OTf)(H_2O)(L^2)_2]^{2+}$ (Ln = La, Gd) with a tridentate mode of coordination for L^2 and one pendant P_bO group on each ligand. For Er dimeric structures, $[Er_2(OTf)_4(H_2O)_2(L^2)_2]^{2+}$ and $[Er_2(OTf)_4(EtOH)_2(L^2)_2]^{2+}$ are formed in which L^2 bridges between the two metal centres.

The La crystal was poorly diffracting, resulting in unsatisfactorily high *R*1 and w*R*2 values, but the dataset was of good enough quality to show that the complex formed is isostructural with the Gd derivative. The molecular geometries of the lanthanum and gadolinium complexes are dodecahedral (S = 0.67 and 0.81 respectively) and the structure of $[La(OTf)(H_2O)(L^2)_2]^{2+}$ is shown as an example in Fig. 5. Average bond distances and angles are summarised in Table 1.

The third P_bO is not bonded to the metal and it might be expected that this is reflected in a shorter P_b=O distance. As can be seen from Table 1 the P=O distances in the pendant arms are only slightly shorter than P=O(Ln). This is due to strong secondary interactions involving the pendant PO groups. In both the La and Gd complexes there is hydrogen bonding with the lattice water/ethanol. In the La complex the P=O….O (lattice water) is 2.745 Å compared with the sum of Van der Waals radii of 3.207 Å, whilst in the Gd complex there is strong H-bonding to lattice ethanol with O…O of 2.653 Å.

The coordinated triflate is weakly H-bonded to the coordinated water molecule with O(5)…..O(9) distances of 2.886 Å and 2.878 Å for the La and Gd complexes respectively, both significantly below the sum

Table 1
Average bond distances (Å) and angles (°) in complexes of L^1 and L^2.

	L^1		L^2			
	Sc	Nd	La	Gd	Er (H2O)	Er (EtOH)
Ln-O(P_a) (κ^3)	2.08 (7)	2.45 (4)	2.46 (2)	2.37 (2)	2.294 (2)	2.2436 (12)
Ln-O(P_b) (κ^3)	2.08 (4)	2.39 (3)	2.46 (3)	2.36 (4)	2.243 (2)	2.23(2)
Ln-O (P μ-κ^1)					2.225 (2)	2.2164 (14)
Ln-O (OTf)		2.54 (2)	2.632 (3)	2.611 (2)	2.351 (2)	2.3440 (15)
Ln-O (EtOH)						2.3908 (14)
Ln-O (H_2O)		2.55 (2)	2.535 (3)	2.400 (2)	2.319 (3)	
P_a=O (κ^3)	1.52 (3)	1.495 (4)	1.50 (2)	1.500 (3)	1.504 (2)	1.5044 (13)
P_b=O (κ^3)	1.52 (3)	1.504 (4)	1.50 (2)	1.499 (2)	1.507 (3)	1.505 (4)
P=O (μ-κ^1)					1.514 (2)	1.5072 (15)
P=O (non coordinated)			1.496 (10)	1.496 (3)		
P_a-O-Ln	144 (2)	151 (5)	157(9)	154 (3)	139.2 (2)	153.78 (8)
P_b-O-Ln	144 (5)	156 (3)	152(6)	155 (5)	149(3)	153(2)
P—O—Ln (μ-κ^1)					147.6 (2)	164.40 (10)
Average angle around P_a	109 (5)	109 (4)	109(5)	109 (4)	109(3)	109(4)
Average angle around P_b	109 (3)	109 (3)	109(5)	109 (4)	109(3)	109(2)
Average angle around P (μ-κ^1)					109(2)	109(2)
Average angle around non coordinated P			109(5)	109 (4)		

of the Van der Waals radii of 3.04 Å respectively [16]. The S—O bond lengths within the coordinated triflate are essentially the same for both La and Gd complexes and reflect these interactions, with S—$O_{(terminal)}$ = 1.433 Å, S—O…H_2O = 1.450 Å and S—O—Ln = 1.452 Å.

The Er complexes were crystallised containing the cation in two differently solvated forms: $[Er_2(OTf)_4(H_2O)_2(L^2)_2]^{2+}$, and $[Er_2(OTf)_4(EtOH)_2(L^2)_2]^{2+}$, Both are binuclear, with two oppositely oriented bridging μ-κ^3,κ^1 L^2 ligands. Each metal is coordinated to seven oxygen atoms, one from the solvent molecule, two from monodentate triflate ions and four from the phosphine oxide groups: three chelating with the third P_bO arm bridging between the two metals. The binuclear structure of the aquo complex is shown in Fig. 6.

The coordination geometry about each metal is a distorted pentagonal bipyramid (S = 0.59) as shown in Fig. 7. The apical oxygen atoms are from one of the κ^3 chelating and the κ^1 bridging PO groups. The $O_{(apical)}$ – Er – $O_{(apical)}$ angle is 174.42° in the H_2O coordinated complex and 178.34° in the ethanol coordinated complex. The angles in the pentagonal plane range from 69.64° to 75.73° with averages of 72.78° (H_2O) and 72.43° (EtOH). The angles subtended by the apical atoms and those in the equatorial plane range from 82.9° to 98.1° (H_2O) and 82.4° to 102.5° (EtOH), with an average of 90.00° in each case.

In the water coordinated complex, the Er-O-P_b angles for the side arm groups are wider than those for the P_aO group. In this case the coordination of central PO appears somewhat more strained with an Er—O—P angle of 139.19° compared with angles of 151.1° and 147.5° for the side arm groups and 147.6° at the bridging PO. This in turn is reflected in the weakest PO-Er interaction: the central P_aO group has the longest Er-O distance of 2.294 Å compared with 2.266 Å and 2.219 Å for the other chelating groups and 2.225 Å for the bridging phosphine oxide. This apparent strain in the chelating portion of the ligand is probably due to the increased congestion in the coordination sphere of the smaller Er^{3+} ion.

In the ethanol coordinated complex, however, the κ^3 chelating ligand does not show this strain. Here, the coordination of central P_aO has an Er—O—P angle of 153.76° and the angles for the side arm groups are similar at 151.80° and 153.96°. The bridging PO has the widest angle at 164.40°. The PO- Er interactions in this complex do not appear to be affected by strain in the chelating group, but show differences between axial and equatorial positions: The two axial Er-O bonds are 2.215 Å and 2.216 Å, whereas the two Er-O(P) bonds within the central pentagonal plane are slightly longer at 2.244 Å and 2.248 Å.

The water coordinated complex has the two coordinated triflate ions adjacent to each other in the central pentagonal plane of the complex. The coordinated water molecule lies between one of the triflates and the equatorial P_bO group of the chelating ligand. There is an intramolecular H-bond to one of the coordinated triflates, and an intermolecular H-bonded to a third triflate. This may be the origin of the strain in the

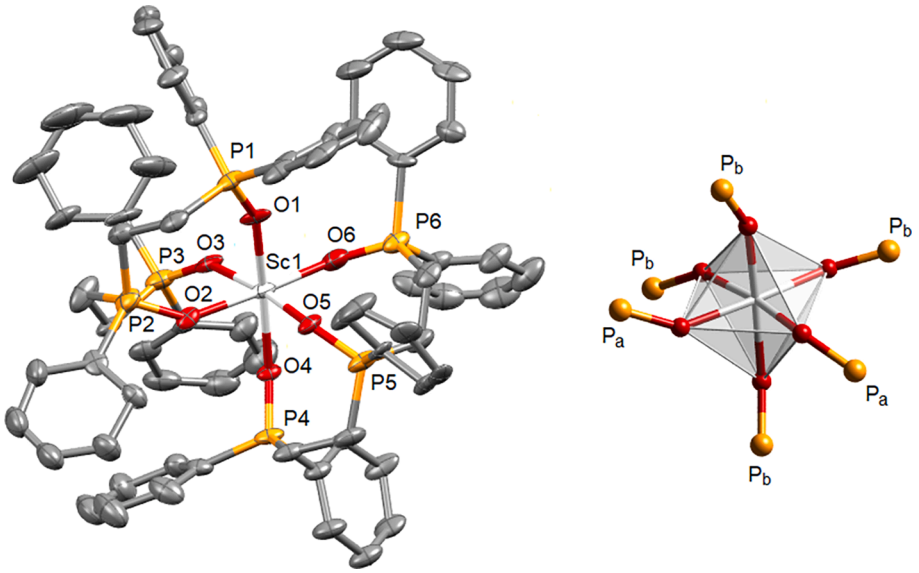

Fig. 3. The octahedral structure of $[Sc(L^1)_2]^{3+}$ Thermal ellipsoids are drawn at 50 % probability. Hydrogen atoms omitted for clarity.

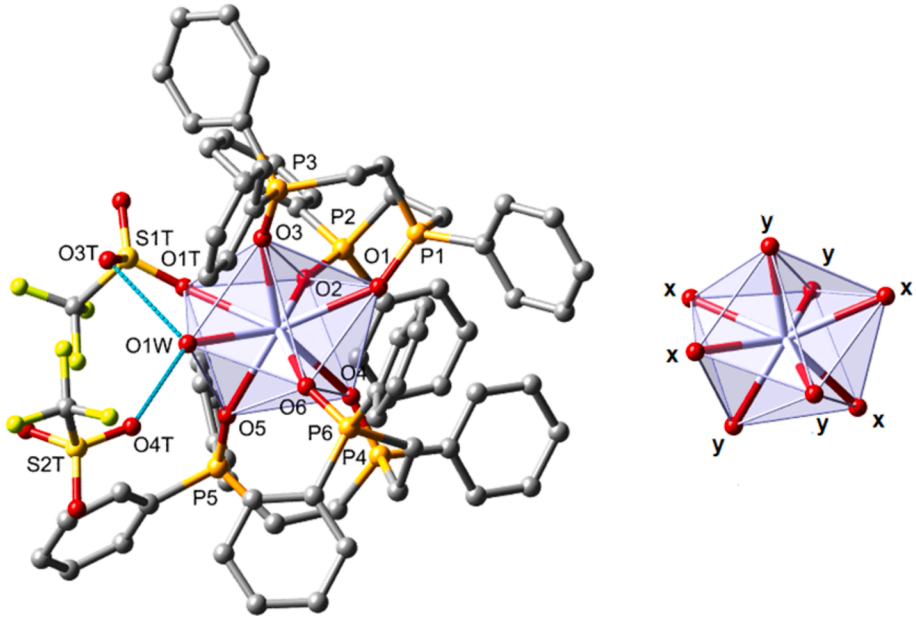

Fig. 4. Left the structure of one of the two $[Nd(OTf)(H_2O)(L^1)_2]^{2+}$ cations in the asymmetric unit. Hydrogen atoms, triflate anions and lattice solvent molecules omitted for clarity. Hydrogen bonding of the coordinated water molecule is shown by the blue dashed line. Right the labelling of the dodecahedron.

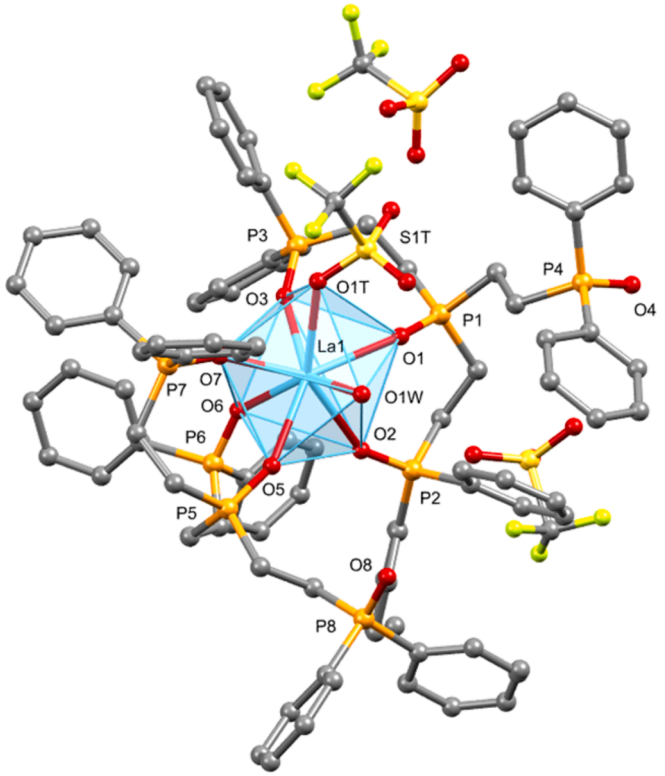

Fig. 5. The dodecahedral structure of $[La(OTf)(H_2O)(L^2)_2](OTf)_2$. Hydrogen atoms and lattice solvent molecules omitted for clarity.

chelating group. In the ethanol coordinated complex, the coordinated triflates are separated by the coordinated ethanol molecule which H-bonds to one of them. There is no intermolecular H-bond to a third triflate.

The Ln-O distances decrease from La to Er as expected as a result the lanthanide contraction. The plots of Ln-O(P) distance versus the ionic radius (8-coordinate for La and Gd and 7-coordinate for Er) are linear with correlation coefficients above 0.99 and indicate that these distances vary in accord with the lanthanide contraction as shown in Fig. 8. Whilst there is a general trend of decreasing distance the Ln-O(OTf) bond lengths do not correlate as strongly with the ionic radii. This is probably due to the hydrogen bonding also influencing the Ln-O bond distances.

In complexes where the ligands geometry is relatively unconstrained by its structure, Ln—O—P angles approaching 180° are found [18,19] thus minimising unfavourable electrostatic interactions between the positive lanthanide and phosphorus centres. The angles here are narrower, show no pattern in the mononuclear complexes and no difference between the mono- or binuclear complexes.

2.4. Infrared spectroscopy

The infrared spectra should provide a means of establishing the coordination mode of the triflate ions, however in practice assignments are complicated by the presence of overlapping bands from the ligand and the presence of the free ion in all of the structures. Some assignments have been made by comparison of the absorptions of the free ligand, their complexes and those of the uncoordinated triflate anion [20]. The PO shifts on coordination to the metal from around 1170 cm^{-1} to 1125 cm^{-1} whilst strong bands from the free triflate ion are observed at 1274 cm^{-1} ($\nu_{as}SO_3$), ~1250 cm^{-1} (ν_sCF_3), 1140 cm^{-1} ($\nu_{as}CF_3$) and 1030 cm^{-1} (ν_sSO_3). The observation of bands from coordinated triflate are more difficult to identify due to mixing and coincidences of stretching modes [21]. The reported coordination shift in $\nu_{as}(SO_3)$ from around 1280 cm^{-1} to 1380 cm^{-1} is not observed here for the crystallographically confirmed coordinated trifate ions. In these cases a peak at about 1300 cm^{-1} is observed as a shoulder on the 1280 cm^{-1} absorption from the free ion.

2.5. Solution properties

The solution properties of the complexes have been investigated by ^{19}F and ^{31}P NMR spectroscopy.

The ^{31}P NMR spectra of $[Sc(L^1)_2](OTf)_3$ in CD_3CN show dynamic behaviour. Three singlets in a 1:1:1 ratio at 57.6, 49.7 and 48.3 ppm are observed at −40 °C. The peaks were assigned by comparison with the order of the chemical shifts in the free ligand and their variable

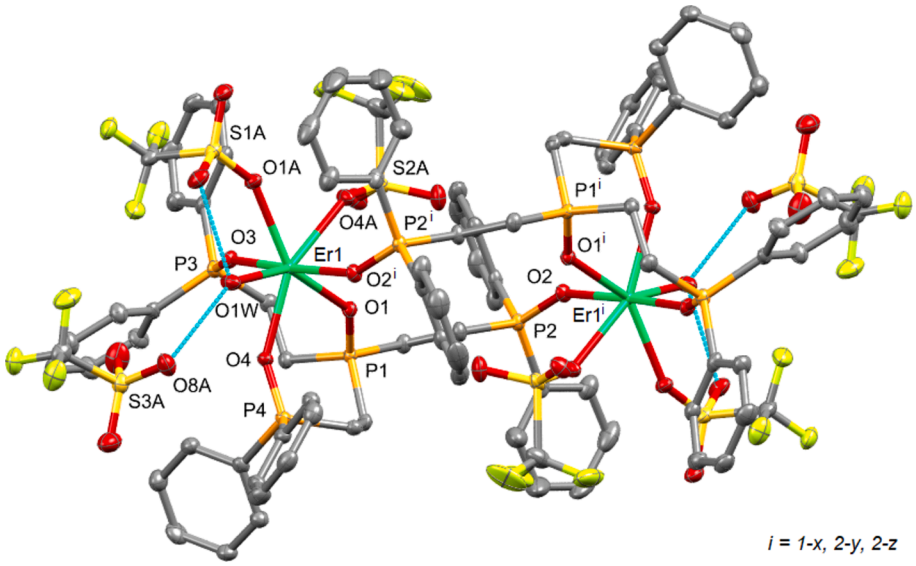

Fig. 6. The structure of $[Er_2(OTf)_4(H_2O)_2(L^2)_2](OTf)_2$. Thermal ellipsoids are drawn at 50% probability. Hydrogen atoms omitted for clarity. Hydrogen bonding of the coordinated water molecule is shown by the blue dashed line.

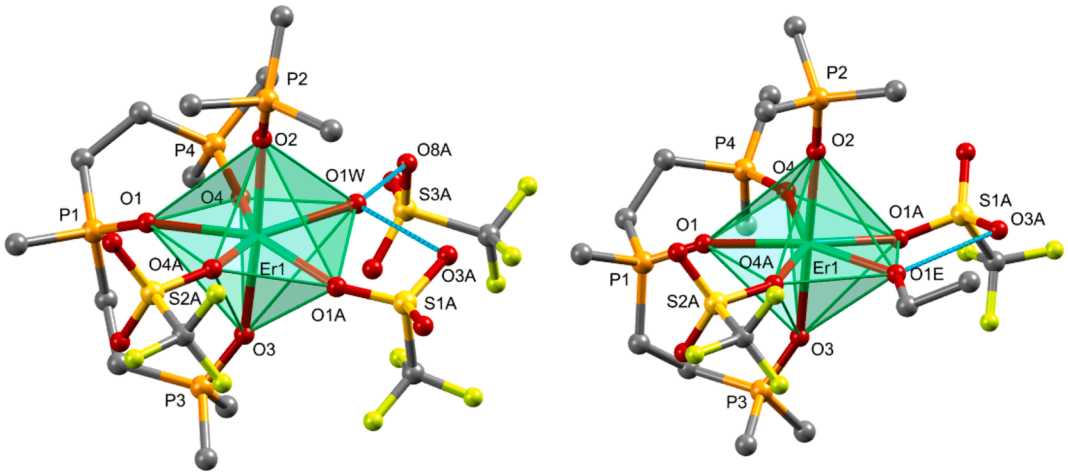

Fig. 7. The coordination geometry about Er in $[Er_2(OTf)_4(H_2O)_2(L^2)_2]^{2+}$ (left) and $[Er_2(OTf)_4(EtOH)_2(L^2)_2]^{2+}$ (right). Hydrogen bonding of the coordinated water and ethanol molecules is shown by the blue dashed line.

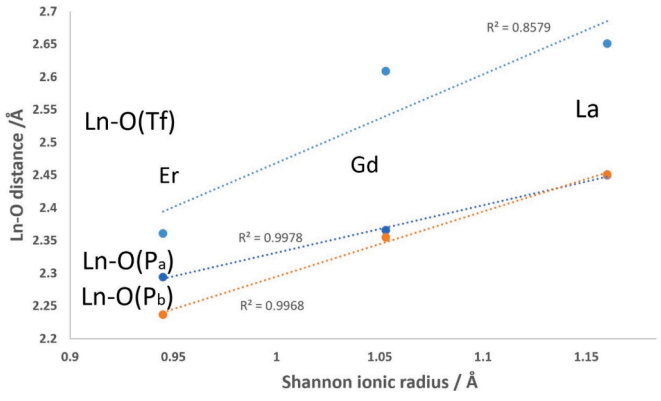

Fig. 8. Ln-O bond distances versus ionic radius 8-coordinate (La, Gd) and 7-coordinate (Er) in complexes of L^2.

temperature behaviour which is discussed below. The resonance at 57.6 ppm is assigned to P_a whilst the signals at 49.7 and 48.3 are due to P_b. The value of $|^3J_{PP} + {}^4J_{PP}|$ must be below 15 Hz (the linewidth at this temperature) which given the relatively large value of $^3J_{PP}$ in the free ligand (the parameters for which are P_a (t) δ 40.9 ppm, P_b (d) δ 31.6 ppm $^3J_{PP}$ = 50 Hz) implies that the $^3J_{PP}$ and $^4J_{PP}$ pathways have opposite signs thus reducing the overall observed magnitude of $|^3J_{PP} + {}^4J_{PP}|$. The reduced coupling on coordination to a metal centre has been previously observed in coordination complexes in phosphines [22] and phosphine oxides [23] and attributed to differing signs of the coupling pathways. On warming the solution, the signal from P_a remains relatively sharp whilst those from the P_b atoms broaden. At 80 °C in CD_3CN and 90 °C in CD_3NO_2 the P_b signals coalesce into a single broad peak indicating exchange between the inequivalent P_b sites. The process is reversible with an identical ^{31}P NMR spectrum obtained on cooling to ambient temperature. The variable temperature spectra in CD_3CN are shown in Fig. 9. The solution structure in which the P_b atoms are inequivalent is shown in Fig. 10 is the same as the found in the solid state. There is no exchange between the complex and free ligand in CD_3NO_2 at 90 °C indicating that in this solvent exchange process is intramolecular. The

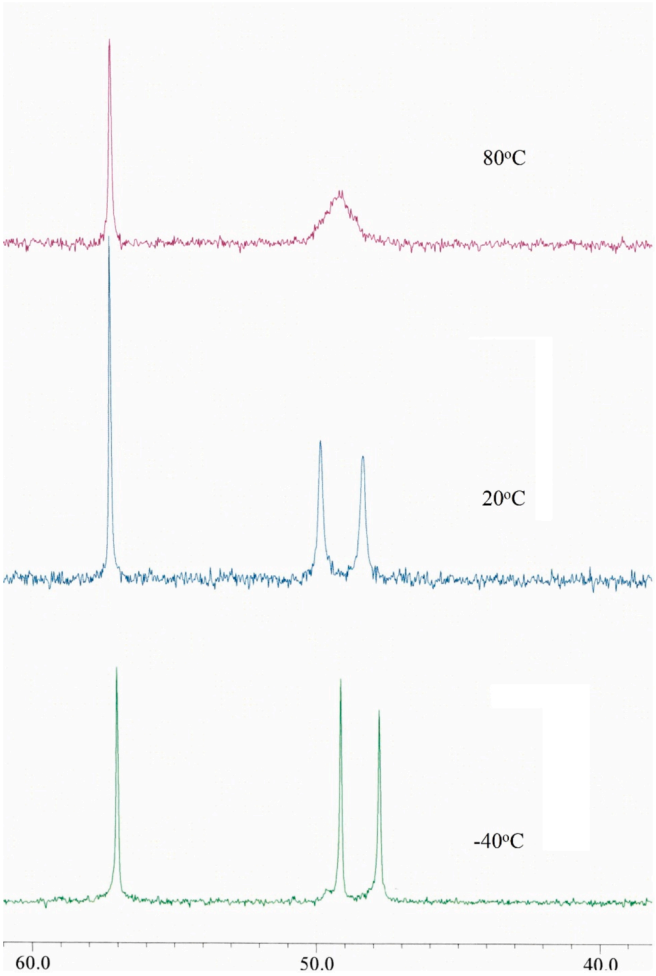

Fig. 9. The variable temperature 161 MHz ^{31}P NMR spectra of the $[Sc(L^1)_2](OTf)_3$ in CD_3CN.

ambient temperature ^{31}P NMR spectra of the Nd, Ho and Yb complexes were difficult to obtain due to a combination of low solubility and excessive line broadening. The spectra show 2 broad signals in a 2:1 integrated ratio (Nd: δ 107.9 (1P, P_a) and δ 110.6 (2P, P_b); Ho: δ–63.3 (1P, P_a) and 38.3(2P, P_b); Yb: δ −6.0 (1P, P_a) and δ 39.5 (2P, P_b)) which indicates a similar coordination of all three PO groups and a similar rapid exchange of different P_b environments.

The spectra for the Nd complex are shown in Fig. S8 in the supplementary information.

All the complexes of L^2 show a similar dynamic behaviour on the NMR timescale indicative of exchange between bound P_bO groups as discussed above, together with additional exchange between the free and coordinated arms of the ligand. The variable temperature ^{31}P NMR spectra of the scandium complex in CD_3CN are shown in Fig. 11. At −40 °C four resonances are seen; P_aO and pendant $P_{b1}O$ as doublets at δ 69.7 and 31.1 ppm $^3J_{PaPb1}$ = 43 Hz respectively and two inequivalent $P_{b2}O$ and $P_{b3}O$ observed as singlets at δ 49.9 and 48.6 ppm. The presence of three inequivalent P_b atoms indicates a similar geometry to the L^1 complexes as indicated in Fig. 10. The chemical shift assigned to P_{b1} is similar to that found for the free ligand whilst significant coordination shifts are seen for P_a, P_{b2} and P_{b3}. As found for the scandium complex of L^1 the P—P coupling is much reduced on coordination with $|^3J_{PP} + {}^4J_{PP}|$ coupling not visible between the coordinated P atoms whilst the coupling between P_a and the free P_{b1} group is similar to that found in L^2 itself.

The ^{19}F NMR spectra showed a single sharp line at around −79 ppm due to the free triflate ion with no sign of interaction with the metal complex in solution at any temperature.

On warming the solution, signals from the P_b atoms broadened at 20 °C and at 80 °C coalesce to a broad peak. We were unable to observe the rapid exchange limit as 80 °C is the high temperature limit for the solvent. The J-J splitting pattern observed for P_a varied with temperature as shown in the inset of Fig. 11. At −40 °C it is a doublet coupling to P_{b1} with no resolved coupling observed with the coordinated P_b atoms. At higher temperature a 1:3:3:1 quartet ($|^3J_{PP} + {}^4J_{PP}|$ = 17 Hz) was initially seen due to the averaging of the coupling between the relatively high value of 43 Hz ($^3J_{PaPb1}$) and the much lower (<20 Hz – the linewidth of the P_a signals at −40 °C) of the $P_{b2,3}$ signals. As the exchange becomes faster the apparent magnitude of the coupling within the quartet is further reduced ($^3J_{PP}$ = 13 Hz) due to a greater contribution to the coupling from the low J value of the coordinated ligands.

The lanthanum complex shows similar variable temperature behaviour and the spectra are shown Fig. 12. At 80 °C the rapid exchange limit spectrum was seen with a 1:3:3:1 quartet for P_a (δ 59.1 ppm J_{PP} 13 Hz) and a doublet for P_b (δ 39.0 J_{PP} 13 Hz). At −40 °C the exchange between free and coordinated P_b was slower but did not resolve into two separate signals, showing broad peaks at 40.5 ppm ($W_{1/2}$ = 600 Hz) and 58.5 ppm ($W_{1/2}$ = 45 Hz) for P_a. The exchange process for La is faster than that observed for Sc probably as a result of the weaker binding of the ligand to the larger La^{3+} ion.

The spectra for the binuclear Er complex were much more difficult to obtain due to the low solubility of the complex which necessitated extended accumulation times. At 30 °C the spectrum shows two relatively sharp signals ($W_{1/2} \approx 300$ Hz) in a 1:1 ratio, at δ −17.5 and −31.1 ppm and a much broader peak ($W_{1/2} \approx 1000$ Hz) due to 2P atoms, at

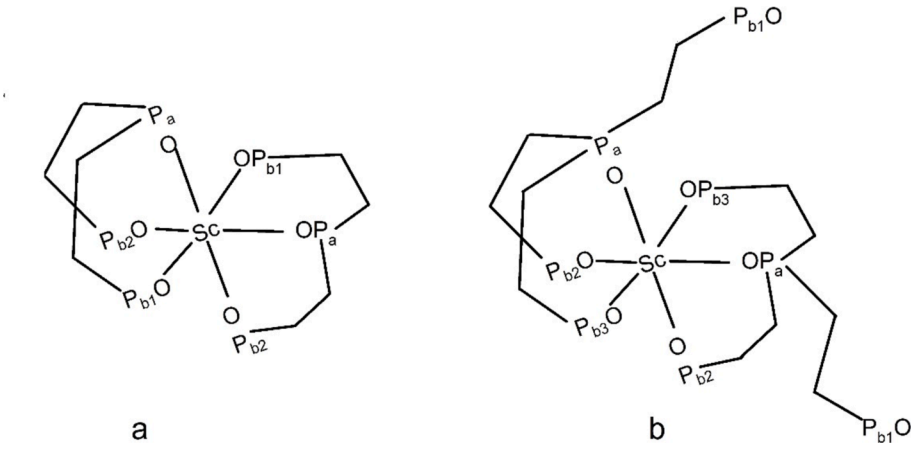

Fig. 10. The structures of a the $[Sc(L^1)_2]^{3+}$ and b the $[Sc(L^2)_2]^{3+}$ ions in solution.

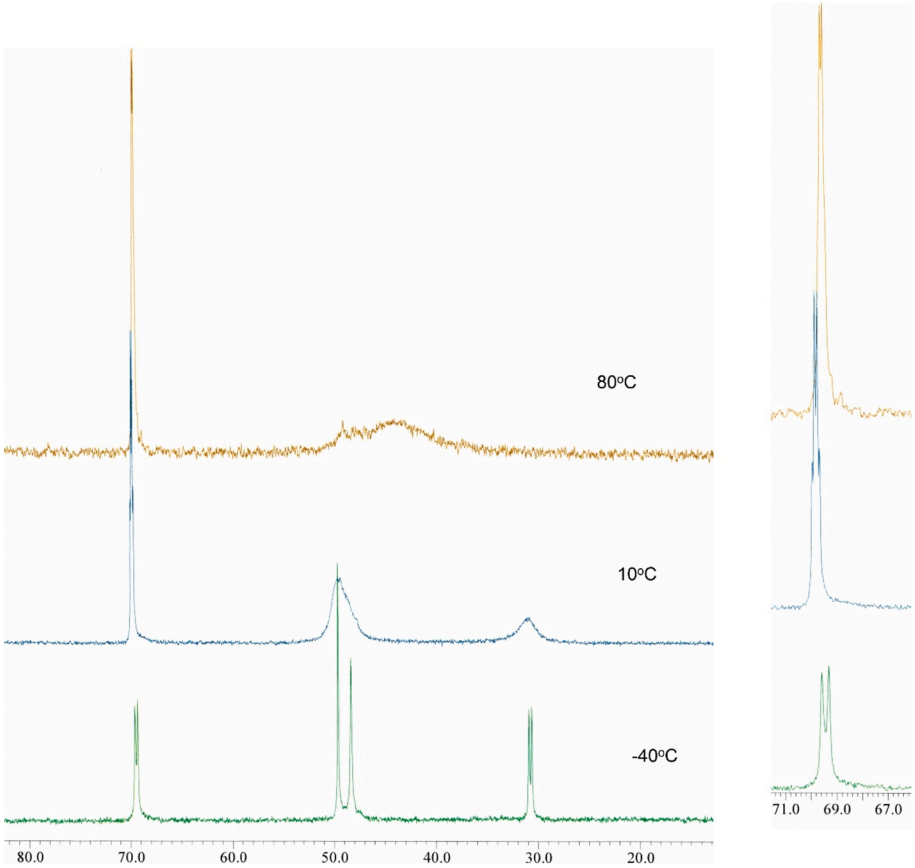

Fig. 11. The 161 MHz ^{31}P NMR spectra of $[Sc(L^2)_2](OTf)_3$ in CD_3CN (the inset to the right shows expansions of the P_a signal).

about δ −45 ppm which are consistent with the dimeric structure found for the solid state. Using the same terminology as with the mononuclear complexes above, we tentatively assign these peaks as P_a at δ −17.5 ppm, the bridging P_{b1} to the −31.1 ppm and the two P_{b2} atoms to the broad signal at −45 ppm. In the crystal structure the two P_{b2} atoms are inequivalent, one being in an axial position and the other equatorial. The broad signal observed indicates exchange between the two environments on the NMR timescale. At 80 °C this exchange is more rapid and P_{b2} peak sharpens ($W_{1/2} \approx 700$ Hz) whilst the line widths of the other two signals remained unchanged. It is worth noting here that, as for all the complexes studied, the ^{19}F spectra show a single peak at about −80 ppm at all temperatures, similar to the position of free triflate. One possible explanation is rapid exchange between the free and coordinated triflate. However, if this were the case some paramagnetic shifts would still be expected which were not observed. It is more likely that in solution the coordinated triflate ions seen in the solid state have been displaced by CD_3CN.

2.6. Catalytic properties

The catalytic properties of representative complexes (the Sc, Nd and Er complexes of L^1 and the Sc, La, Nd, and Er complexes of L^2) were assessed towards the catalytic alkenylation of activated aromatics [24] in CH_3NO_2 at 80 °C.

An equimolar solution of 1,4-dimethoxybenzene and phenylacetylene, with naphthalene as an internal standard, was treated with about 5 mol% of representative complexes of L^1 and L^2 at 80 °C and monitored by GC mass spectrometry for the presence of *trans*-2,5-dimethoxystilbene as shown in Scheme 2.

After 2 weeks at 80 °C there was no sign of the above reaction for the complexes of L^1 whilst only the Nd and Er complexes of L^2 led to the formation of very small amounts of the alkenylation product. In all cases (including stock solutions containing no lanthanide complexes) slow oxidative dimerisation of phenylacetylene occurred giving *trans*-PhC(O)CH=CHC(O)Ph, identified by its mass spectrum (*m/z* 236 (20 %) due to M^+ and *m/z* 105 (100 %) due to $[PhCO]^+$) which gives an exact match to the library spectrum as shown in the supplementary information. The lack of reactivity for the scandium complexes is not surprising in view of the strong binding of the ligand to the metal and the intramolecular processes involved in exchange of the inequivalent phosphorus environments. For the complexes of the other metals access to the primary coordination sphere might be expected to be easier due to the presence of weakly coordinating triflate ions. However, for the majority of the complexes examined this is insufficient to promote any significant reaction. The dimeric erbium complex was most reactive, but it is not clear that catalysis has occurred with only approximately 2 % conversion to the stilbene after 3 weeks at 80 °C.

2.7. Electrospray mass spectrometry

Electrospray mass spectrometry has previous been used to study complexes of lanthanide triflates with triphenylphosphine oxide [25]. $[Ln(OTf)_3(Ph_3PO)_4]$ showed a variety of species such as $[Ln(Ph_3PO)_6]^{3+}$ $[Ln(Ph_3PO)_5]^{3+}$ and $[Ln(OTf)(Ph_3PO)_5]^{2+}$ which are probably formed as the result of ligand redistribution on the 0.2 s time scale of the electrospray process [26]. This redistribution is favoured by the combination of the labile nature of lanthanide coordination complexes with monodentate ligands and weakly coordinating triflate ions.

Whilst the presence of ions in the gas phase cannot be taken to imply their presence in solution, it might be expected that complexes with multidentate ligands might show less propensity to undergo ligand redistribution during the electrospray process and the resulting mass spectra might better reflect the nature of the species in solution. Thus it was of interest to obtain the ESMS of complexes with the ligands of

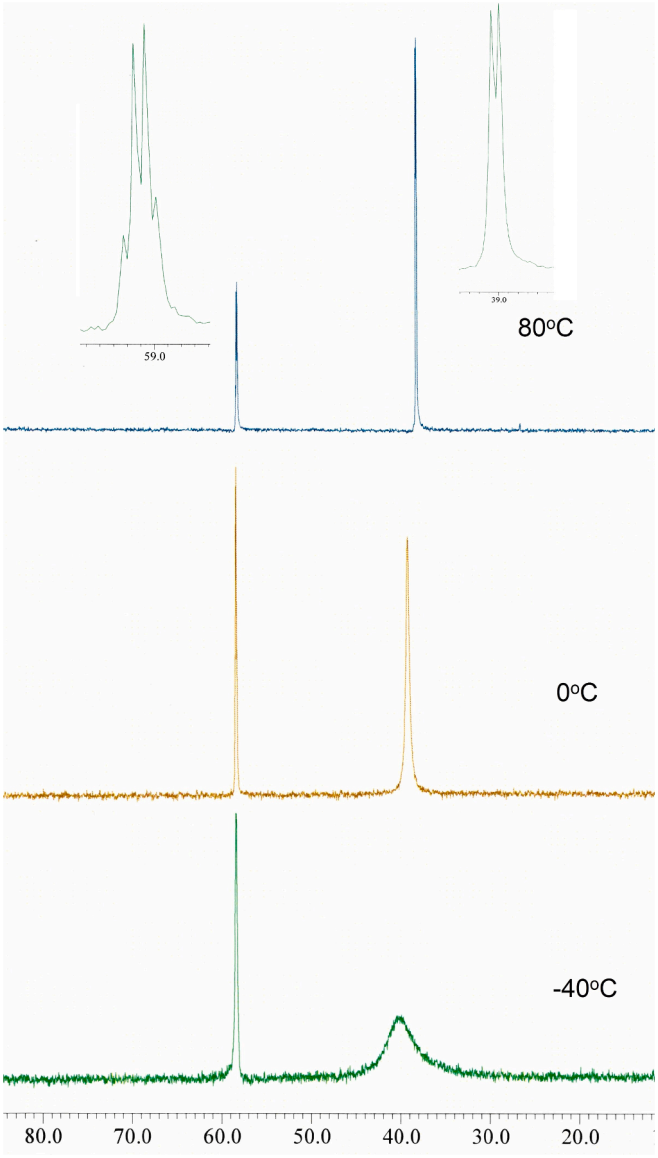

Fig. 12. The variable temperature 161 MHz ^{31}P NMR spectra of [La(OTf)$_3$(H$_2$O)(L^2)$_2$] in CD$_3$CN. The insets show expansions of the spectra at 80 °C The inset shows the expansion of the P$_a$ and P$_b$ signals.

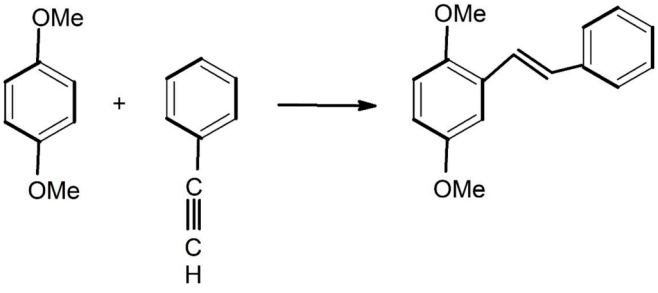

Scheme 2. The reaction of 1,4-dimethoxybenzene and phenylacetylene.

higher denticity studied here.

All spectra were recorded in methanol. The free ligands give the expected peaks corresponding to $[L + H]^+$ and $[L + Na]^+$ as the base peaks for both L^1 and L^2.

Complexes of L^1 with general formula Ln(OTf)$_3$(L^1)$_2$ might be expected to give ions such as $[Ln(OTf)_2(L^1)_2]^+$, $[Ln(OTf)(L^1)_2]^{2+}$ and $[Ln(L^1)_2]^{3+}$due to loss of the weakly coordinating triflate ion. In line with this expectation these ions are observed, although the "parent ion" is generally of low intensity (~5% or lower) and observed only on increasing cone voltage. The base peak for all complexes is due to $[Ln(L^1)_2]^{3+}$ and arises due to loss of triflate from a relatively substitution-stable Ln(L^1)$_2$ core. However, there are ligand redistribution products present in these spectra which give rise to significant peaks assigned as $[Ln(OTf)(L^1)_3]^{2+}$ (~30 %), $[Ln(L^1)_3]^{3+}$ (~45 %) and $[Ln(L^1)_4]^{3+}$ (~20 %).

Whilst the complexes of L^2, of general formula Ln(OTf)$_3$(L^2)$_2$, show similar features to the spectra described above there are significant differences. Here the ligand geometry excludes the possibility of tetradentate coordination to a single metal, but the tridentate mode is clearly established in the solid state. The base peak for the lanthanum complex is due to $[La(OMe)_2]^+$ and whilst the analogous methoxide gives rise to peaks of significant intensity in the spectra of the gadolinium and erbium complexes, the overall intensity is reduced due to the presence of multiple isotopes of these elements. The presence of metal containing ions without attached L^2 implies that its dissociation is favourable in contrast to the complexes of L^1. An intense peak due to $[Ln(OTf)(L^2)_2]^{2+}$ is clearly derived from the solid state structure and $[Ln(L^2)_2]^{3+}$ (60–100 %) being derived from loss of triflate either in solution or in the gas phase. Lower intensity signals are observed from redistribution products; $[Ln(L^2)_3]^{3+}$ (5 – 15 %) being particularly significant. It is possible to account for many of the observed ions by redistribution occurring via solution processes or due to fragmentation/recombination in the gas phase.

Several of the ions observed in the electrospray mass spectra were selected for analysis by tandem mass spectrometry to assess their stability in the gas phase.

As the parent ion in the spectra from complexes of L^1 was of low abundance, we examined the ion $[Ln(OTf)_2(L^1)]^+$ which may be considered as being formed from M – OTf –L. Both the Nd and Ho complexes gave daughter ions corresponding to sequential fluoride ion abstraction from triflate with loss of CF_2SO_3 ($m/z = 130$). Significantly there were no product ions that corresponded to any of the ions observed in the normal ESMS. The results for the $[Ho(L^1)_4]^{3+}$, $[Ho(OTf)_2(L^1)]^+$, $[Ho(OTf)(L^1)_2]^{2+}$ and $[La(L^2)_4]^{3+}$ and $[La(OTf)(L^2)_2]^{2+}$ ions observed in the ESMS are summarised in Scheme 3 and an example of the tandem mass spectrum of the $[La(OTf)(L^2)_2]^{2+}$ ion is shown in Fig. 13.

The homoleptic species such as $[Ln(L^1)_4]^{3+}$ and $[Ln(L^2)_4]^{3+}$ fragment at low energy by successive loss of ligand, ultimately producing $[LnL_2]^{2+}$. Presumably the reduction in steric crowding is the driving force in these fragmentations, and in this regard it is interesting that ions containing 2 or fewer ligands show little tendency to decompose by this pathway. Ions such as $[Ln(OTf)_2L]^+$ and $[Ln(OTf)L_2]^{2+}$ appear to be more robust in the gas phase and require high collision energies to undergo fragmentation.

Fluoride abstraction from triflate by the lanthanide ion is the only decomposition route observed for $[Ho(OTf)_2(L^1)]^{2+}$ whilst this pathway is observed for all the triflate containing ions.

A common mode of fragmentation is either direct loss of diphenylphosphine oxide or fluoride abstraction with loss of $Ph_2P(O)C_2H_4OSO_2CF_3$ followed by sequential loss of $Ph_2P(O)H$. The loss of diphenylphosphine oxide presumably occurs via β-hydrogen transfer from C to P in a pendant ligand arm as indicated in Scheme 4.

The β-hydrogen atoms on the coordinated sections of the ligand are less likely to transfer as they are on average further from the phosphorus, at least in the solid state structures. The crystal structures of [La(OTf)$_3$(L^2)$_2$] and [Gd(OTf)$_3$(L^2)$_2$] show the presence of pendant ligand arms in the solid state and presumably this feature is either retained in some of the gas phase structures or is readily achieved.

Some support for this is found in the observation of the fragmentation of the molecular ion in L^2. Here sequential loss of three molecules of $Ph_2P(O)H$ from the parent ion $[OP(C_2H_4P(O)Ph_2)_3 + H]^+$ (20 %) occurs

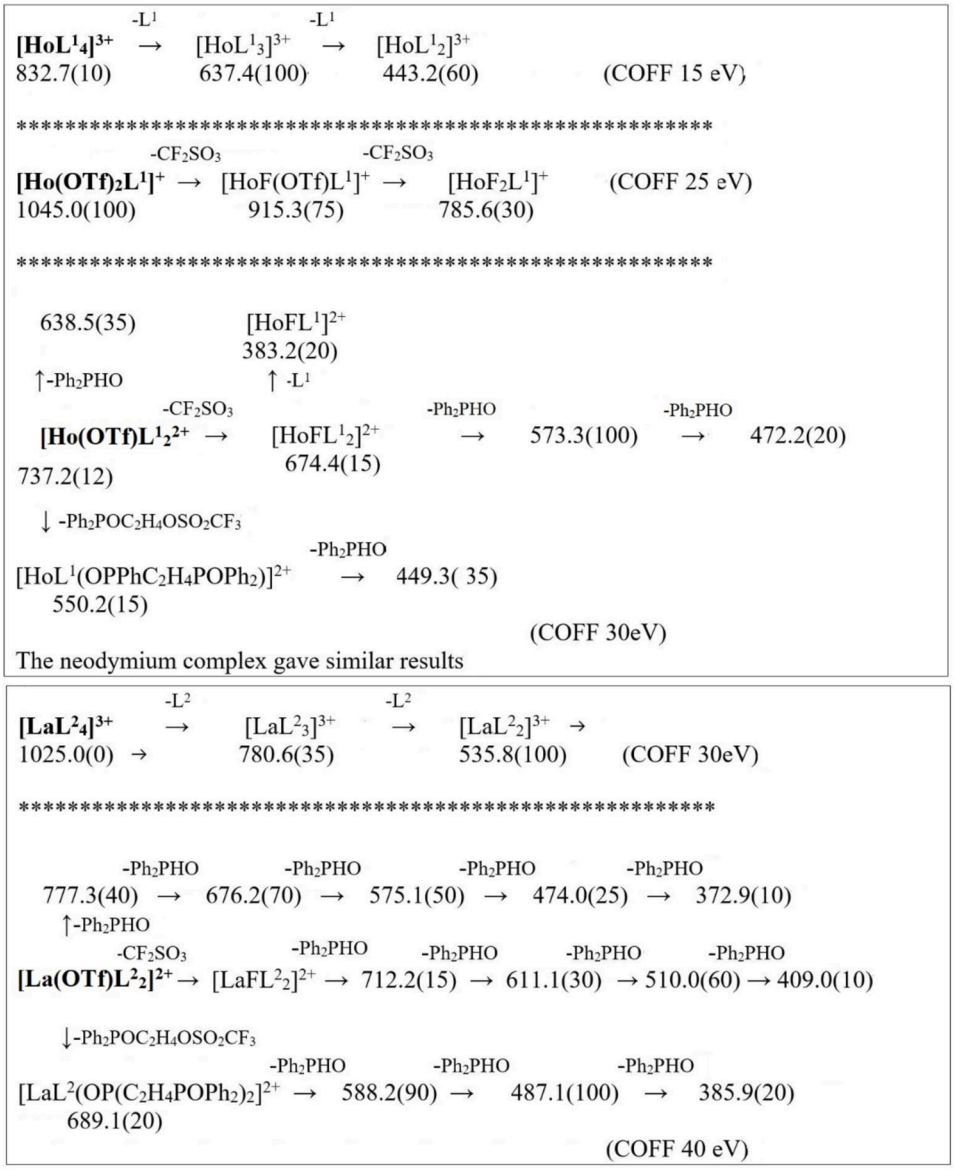

Scheme 3. The tandem mass spectra of the $[Ho(L^1)_4]^{3+}$, $[Ho(OTf)_2(L^1)]^+$, $[La(L^2)_4]^{3+}$, and $[La(OTf)(L^2)_4]^{2+}$ parent ions.

giving product ions at $m/z = 533.4(40\ \%)$, 331.2(100 %) and 129.2(3 %) due to $[OP(C_2H_4P(O)Ph_2)_2C_2H_3 + H]^+$, $[OP(C_2H_4P(O)Ph_2)(C_2H_3)_2] + H]^+$ and $[OP(C_2H_3)_3 + H]^+$respectively. Some P to C oxygen transfer is also apparent during the fragmentation process. Thus an intense peak at $m/z = 489.2(65\ \%)$ is due to loss of $Ph_2P(O)C_2H_4OH$ from the parent ion. This ion also undergoes sequential loss of $Ph_2P(O)H$ to give signals at $m/z = 287.1(75\ \%)$ and 176.1(1 %).

Fragmentation via loss of the triflate ester, $Ph_2P(O)C_2H_4OSO_2CF_3$, is an unusual mode which nonetheless occurs to a significant extent. Approximately 20 % of $[Ho(OTf)(L^1)_2]^{2+}$ and 40 % of $[La(OTf)(L^2)_2]^{2+}$ decompose in this way.

3. Conclusion

Complexes of scandium and lanthanide triflates with $PhP(O)(C_2H_4P(O)Ph_2)_2$ (L^1) and $P(O)(C_2H_4P(O)Ph_2)_3$ (L^2) have been prepared have ionic structures in which the ligands act as tridentate ligands in both solid state and in solution. In solution variable temperature ^{31}P NMR spectroscopy shows the complexes undergo intramolecular fluxional behaviour on the NMR timescale. The complexes show no catalytic activity probably due to the strong coordination of the ligand. The electrospray mass spectrometry of the complexes show that apart from the scandium complexes, extensive ligand redistribution occurs in the gas phase which is not observed in solution and thus the solution and gas phase structures are very different. Unusual decomposition pathways via loss of diphenylphosphine oxide and $Ph_2P(O)C_2H_4OSO_2CF_3$ occur in the gas phase.

4. Experimental

4.1. X-ray crystallography

Crystallographic data collections were undertaken at 100(2) K. Datasets were collected on a Rigaku FRE+ ($[Sc(L^1)_3](OTf)_3$, $[Er_2(OTf)_4(EtOH)_2(\mu\text{–}L^2)_2](OTf)_2$ using Mo Kα radiation, or a Rigaku 007HF ($[La(OTf)(H_2O)(L^2)_2](OTf)_2\ H_2O$ solvate) using Cu Kα radiation. Data collection and integration were performed using CrysAlisPro [27], the structures were solved in Olex2[28] using SHELXT [29], and refined using SHELXL-2018[30]. Data for the remaining samples $[La(OTf)(H_2O)(L^2)_2](OTf)_2$ EtOH solvate, $[Nd(OTf)(H_2O)(L^1)_2](OTf)_2$, $[Er_2(OTf)_4(H_2O)_2(L^2)_2](OTf)_2$, $[Gd(OTf)(H_2O)(L^2)_2](OTf)_2$ were collected on a Bruker Nonius Kappa APEXII diffractometer using

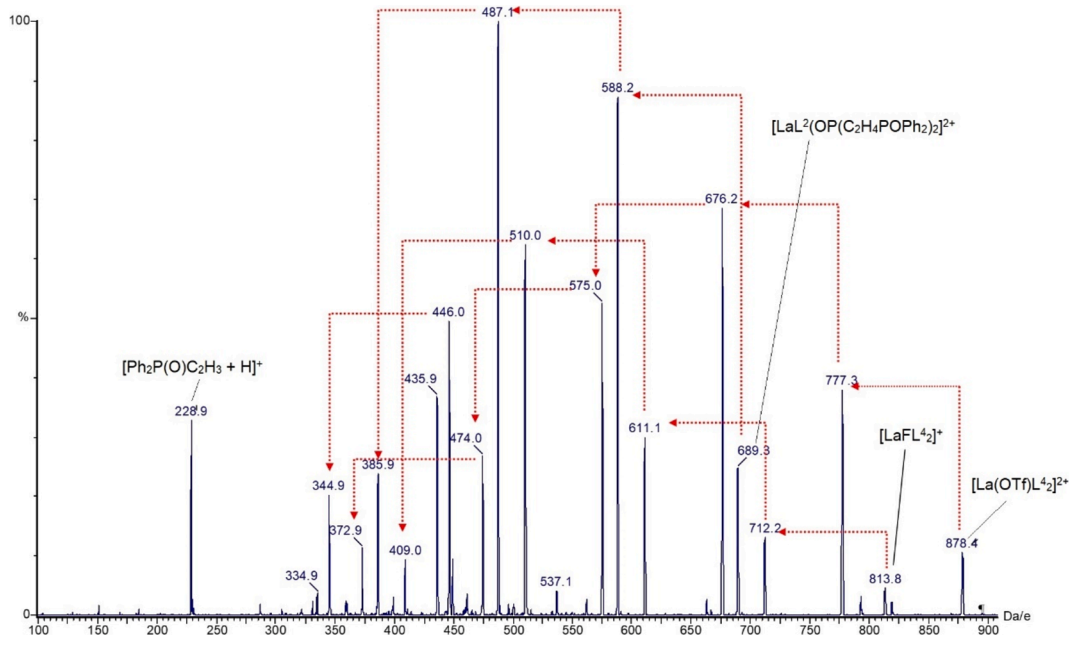

Fig. 13. The Tandem mass spectrum of $[La(OTf)(L^2)_2]^{2+}$. The red arrows indicate successive loss of Ph_2PHO.

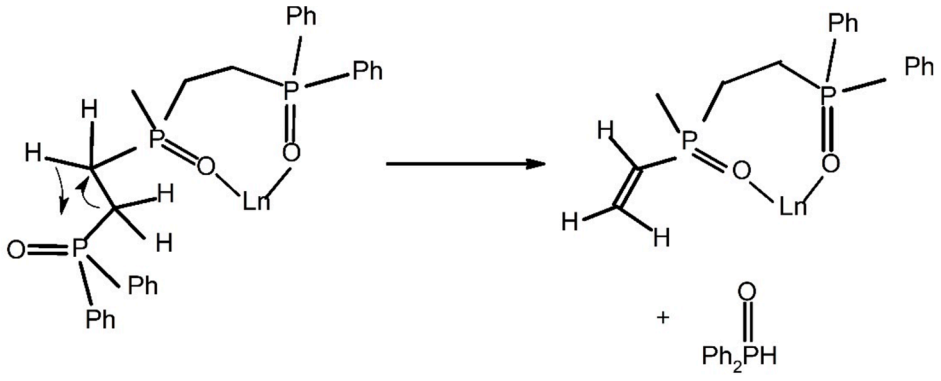

Scheme 4. The loss of diphenylphosphine oxide from a pendant ligand arm in complexes of L^1 and L^2.

previously described procedures [31–34]. Structures were solved using direct methods (SHELXS) [35], and refinement was by full-matrix least-squares on F^2 data using SHELXL-2013 [35] from within the WinGX suite of software [36]. Molecular graphics were generated using Mercury [37].

All non-hydrogen atoms of the complex lanthanide cations, triflate anions, and full occupancy atoms of solvent molecules were refined anisotropically. Aliphatic and aromatic hydrogen atoms were included at their geometrically estimated positions. Hydroxyl hydrogen atoms and hydrogen atoms belonging to water molecules were located in the difference map where possible, and ethanol hydroxyl hydrogen atoms were included at geometrically estimated positions when they could not be located. Disorder of the triflate anions and solvent molecules of crystallisation was common, and disorder of ligands or entire complex cations was observed in $[La(OTf)(H_2O)(L^2)_2](OTf)_2\ H_2O$ solvate and $[Sc(L^1)_3](OTf)_3$, respectively. Details of how the disorder was modelled may be found in the individual cifs. In the cases of $[La(OTf)(H_2O)(L^2)_2](OTf)_2$ (EtOH solvate), $[Nd(OTf)(H_2O)(L^1)_2](OTf)_2$, and $[Gd(OTf)(H_2O)(L^2)_2](OTf)_2$, the solvent disorder could not be modelled and a solvent mask was applied.

Crystallographic data for the structures in this paper have been deposited with the Cambridge Crystallographic Data Centre as supplementary publication numbers CCDC numbers 2377772–2237778. Copies of the data can be obtained, free of charge, on application to CCDC, 12 Union Road, Cambridge CB2 1EZ, UK (Fax: +44(0)-1223–336033 or deposit@ccdc.cam.ac.uk).

NMR spectra were recorded on a JEOL ECX 400, approximately 20 mg of solid in 1 mL of the appropriate deuterated solvent. Infrared spectra were recorded with a resolution of ± 1 cm^{-1} on a Thermo Nicolet Avatar 370 FT-IR spectrometer operating in ATR mode. The samples were compressed onto the optical window and spectra recorded without further sample pre-treatment.

The ligands were prepared by oxidation of a suspension of the corresponding phosphine with hydrogen peroxide in acetone. Electrospray mass spectra were recorded on a either a Waters ZQ-4000 or a Micromass Quattro II for the MS/MS measurements. Samples in methanol solution were loop injected into a flow of 1:1 methanol: water running at 40 μL min^{-1} into the electrospray capillary. Nebulisation was pneumatically assisted by a flow of $N_{2(g)}$ at 15 L min^{-1} and a drying gas of $N_{2(g)}$ at 100 L min^{-1} warmed by a source temperature of 80 °C. The spray voltage was 3.5 kV and the cone voltage varied between 20 V and 90 V depending on the mass and charge of the ions of interest. For tandem mass spectra, $Ar_{(g)}$ at a pressure of $2x10^{-3}$ mbar was introduced into the collision chamber (termed quadrupole 2 or Q2); ions formed during the

ES process and mass selected for individual analysis by the first quadrupole (Q1), were accelerated through this region of relatively high pressure by a voltage termed the collision offset (COFF). The COFF voltage was adjusted to obtain optimal fragmentation for each precursor ion, and the resulting fragment ions analysed by Q3. High resolution mass spectra were recorded on an Agilent 1260 infinity 2 connected to a 6550 iFunnel Q-TOF LC/MS. Gas chromatography mass spectrometry was carried out on a Perkin Elmer Carrus 690 linked to a Clarus SQ8T mass spectrometer.

4.2. Synthesis

L^1. $PhP(C_2H_4PPh_2)_2$ (5.18 g, 9.69 mmol) was suspended in 25 mL acetone and H_2O_2 (4.18 g, 30 % aqueous solution, 37 mmol) in 5 mL acetone was slowly added at such a rate as to maintain steady exothermic reaction. The mixture was stirred overnight, filtered, washed with a little cold acetone and dried at the pump to give 5.53 g (98 %) white powder. NMR $^{31}P(CDCl_3)$ δ 41.83(t), 32.59(d) $^3J_{PP}$ 51.25 Hz Infrared(ATR) ν_{PO} 1190(m), 1172(s) ESMS (Methanol): $[L^1 + H]^+$ *m/z* 583.1722 (theoretical 583.1721) (100 %), $[L^1 + Na]^+$ *m/z* 605.1554 (theoretical 605.1540) (25 %); $[2L^1 + Na]^+$ *m/z* 1187.3193 (theoretical 1187.3283) NMR $CDCl_3$ ^{13}C (100.52 MHz) 132.0(d) $^1J_{PC}$ 101 Hz, 132.0 (s), 130.8(d) J_{PC} 9 Hz, 129.0(d) J_{PC} 12 Hz 29.9(d,d) $^1J_{PC}$ 69 Hz, $^2J_{PC}$ 12 Hz, 15.0 (s) ^1H (399.78 MHz) 7.68(m), 7.45(m) (25H), 2.54(m)(2H), 1.98(m)(2H).

L^2. $P(C_2H_4PPh_2)_3$ (1.01 g, 1.51 mmol) was suspended in 5 mL acetone and H_2O_2(1.26 g 30 % aqueous solution,11.12 mmol) in 5 mL acetone wad added at 0 °C. The suspension initially cleared during addition followed by formation of a copious white precipitate. The mixture was refluxed for 1.5 h and cooled in ice. The white solid was filtered, washed with a little acetone and dried at the pump to give 1.06 g (96 %) NMR $^{31}P(CDCl_3)$ δ 35.35(d), 53.43(q) $^3J_{PP}$ 48.66 Hz Infrared (ATR) ν_{PO} 1197(m), 1175(s) ESMS (Methanol) $L^1 + H]^+$ *m/z* 583.1722 (45 %) (theoretical 583.1721) (100 %), $[L^1 + Na]^+$ *m/z* 735.2105 (100 %) (theoretical 735.2112); $[2L^1 + Na]^+$ *m/z* 1491.3982(15 %) (theoretical 1491.3965).

4.3. Preparation of the complexes

All metal salts were prepared by the reaction of CF_3SO_3H with the appropriate metal oxide. Solutions were evaporated to dryness and the solids recrystallised from ethanol.

4.4. Complexes of L^1

$Sc(OTf)_3{\cdot}6H_2O$ (0.18 g, 0.3 mmol) in 1.5 mL EtOH was added to a suspension of L^1 (0.23 g, 0.4 mmol) in 3.5 mL EtOH and the mixture heated to 80 °C for 4 h during which time the reaction mixture cleared. The volume was reduced to about 1 mL and cooled to room temperature which led to the formation of white crystals. These were filtered, washed with ethanol and dried in vacuo over KOH to give 0.28 g (85 % based on L^1). ESMS (Methanol); $[Sc(OTf)_2(L^1)_2]^+$ *m/z* 1507.1919 (40 %) (theoretical 1507.1885), $[Sc(OTf)(L^1)_2]^{2+}$ *m/z* 679.1219 (60 %) (calculated 679.1182), $[L^1 + H]^+$ *m/z* 583.1882 (100 %) (calculated 583.1721) Infrared (ATR) 3064(w), 2950(w), 1437(m), 1274(s,sh)1251(s), 1244 (s), 1154(s,sh), 1125(s), 1087(s), 1073(s), 1026(s), 997(m), 740(s), 733 (s), 691(s), 675(m).

$Nd(OTf)_3{\cdot}9H_2O$ (0.27 g, 0.22 mmol) in 2 mL methanol was added to a suspension of L^1 (0.12 g, 0.56 mmol) in 2 mL methanol. A clear solution was formed on mixing. Slow evaporation of the remaining clear solution gave a viscous oil which was stirred with water. The resulting lilac solid was filtered and dried at the pump to yield 0.17 g (93 % with respect to L^1). Analysis % $Nd(OTf)_3(L^1)_2(H_2O)$ required (found) C 48.05 (47.87) H3.86(3.69).

Infrared(ATR) ν_{PO} 1142(s) $\nu_{triflate}$ 1257(s), 1223(s) 1027(s) NMR ^{31}P 161 MHz CD_3NO_2 (161 MHz) δ 107.9 (1P) and δ 110.6 (2P) Infrared (ATR) 1592(w), 1484(w),1438(m), 1423(w) 1243(s), 1226(s), 1173(s), 1123(s), 1102(s), 1073(m), 1028(2), 997(m), 733(s), 724(s),692(s).

$Ho(OTf)_3{\cdot}9H_2O$ (0.24 g, 0.29 mmol) in 2 mL methanol was added to a suspension of L^1 (13 g, 0.23 mmol). The clear mixture was heated to 80 °C for 4 h and cooled to room temperature. No solid material formed on cooling and the solution was evaporated to give a viscous resin which was stirred with a small amount of water to give a pale pink solid. This was filtered washed with a little water and dried in vacuo over KOH to give 0.16 g (94 % based on L^1).

Analysis % $Ho(OTf)_3(L^1)_3$ required (found) C53.44(54.12) H4.23 (3.98) NMR ^{31}P 161 MHz CD_3NO_2 δ–63.3 (1P) and 38.3 (2P) Infrared (ATR) 1591(w), 1484(w), 1437(m), 1423(w), 1226(w), 1195(m), 1173 (s), 1121(s), 1103(m), 1072(m), 1028(m), 996(m), 733(s), 723(s), 692 (s).

$Yb(OTf)_3{\cdot}9H_2O$ (0.18 g, 0.23 mmol) in 2 mL methanol was added to a hot suspension of L^1 (0.12 g, 0.21 mmol) in 2 mL methanol. The clear mixture was heated at 80 °C allowed to cool to room temperature overnight. Slow evaporation at room temperature gave an intractable viscous oil which was stirred with a small quantity of water to give a white powder. Drying in vacuo over KOH gave 0.15 g (88 % based on L^1).

Analysis % $Yb(OTf)_3(L^1)_3$ required (found) C53.26(53.77) H4.21 (4.26) NMR ^{31}P 161 MHz CD_3NO_2 δ −6.0 (1P) and δ 39.5 (2P) Infrared (ATR) 1485(w), 1438(m), 1422(w), 1278(w), 1252(w), 1225(w), 1195 (m), 1173(s), 1122(s), 1103(m), 1073(w), 1028(m), 996(w), 740(s), 733 (s), 723(s), 693(s).

4.5. Complexes of L^2

$La(OTf)_3{\cdot}9H_2O$ (0.12 g, 0.16 mmol) in 0.4 mL hot ethanol was mixed with L^2 (0.12 g, 0.17 mmol) in 0.4 mL ethanol. On cooling a small quantity of crystals deposited and were isolated. On standing overnight a colourless solid formed which was filtered washed with a little cold ethanol and dried to give 0.12 g (34 % based on L^2). Analysis % (La $(OTf)_3)_3(L^2)_2$ required (found) C 34.61(34.64) H 2.26(2.93) Infrared (ATR) ν_{PO} 1145(s), $\nu_{triflate}$ 1291(m), 1233(s), 1221(s), 1021(s).

$Gd(OTf)_3{\cdot}9H_2O$ (0.13 g, 0.17 mmol) in 0.4 mL hot ethanol was mixed with L^2 (0.11 g, 0.15 mmol) in 0.4 mL ethanol. On standing overnight a small quantity of colourless crystals formed which were removed from the bulk solution, filtered washed with a little cold ethanol and dried to give crystals suitable for x-ray diffraction. On further standing colourless crystals (which were not suitable for diffraction studies) were obtained which were filtered, washed with ethanol and dried in vacuo to give 0.20 g (32 % based on L^2). Analysis % $(Gd(OTf)_3)_3(L^2)_2$ required (found) C 34.03(33.81) H 2.58(2.60) Infrared(ATR) ν_{PO} 1144(s), $\nu_{triflate}$ 1276(s), 1246(s) 1223(m), 1027(s).

$Er(OTf)_3{\cdot}9H_2O$ (0.11 g, 0.14 mmol) in 0.4 mL hot ethanol was mixed with L^2 (0.12 g, 0.17 mmol) in 0.4 mL hot ethanol. On standing overnight pink crystals formed were filtered washed with a little cold ethanol and dried to give 0.05 g pink crystals.

Analysis % $Er(OTf)_3(L^2)(H_2O)$ required (found) C 39.53(38.06) H 3.24(3.18) Infrared(ATR) ν_{PO} 1144(s), $\nu_{triflate}$ 1276(s), 1246(s) 1223(m), 1027(s).

For the alkenylation reaction between phenylacetylene and 1,4-diemthoxybenzene approximately 0.4 g of the reagents and a similar quantity of naphthalene as internal standard were dissolved in 25 mL nitromethane. The lanthanide complex (~0.003 g) was added to 1 mL of this solution and the mixture heated to 80 °C and monitored by GC- mass spectrometry over three weeks.

CRediT authorship contribution statement

Simon J. Coles: Writing – review & editing, Investigation. **Ann P. Hunter:** Writing – review & editing, Writing – original draft, Methodology, Investigation, Formal analysis. **Sarah J. Fieldhouse:** Writing – review & editing, Writing – original draft, Investigation. **Anthony M.J.**

Lees: Writing – review & editing, Writing – original draft, Investigation, Formal analysis. **Laura J. McCormick McPherson:** Writing – review & editing, Writing – original draft, Investigation. **Andrew W.G. Platt:** Writing – review & editing, Writing – original draft, Project administration, Investigation, Formal analysis, Conceptualization.

Declaration of competing interest

The authors declare that they have no known competing financial interests or personal relationships that could have appeared to influence the work reported in this paper.

Acknowledgements

We are grateful to the EPSRC for the use of the National Crystallography Service at Southampton University [38] and to Dr Alison Davidson of Staffordshire University for assistance with the GC-MS measurements.

Appendix A. Supplementary data

Supplementary data to this article can be found online at https://doi.org/10.1016/j.poly.2025.117395.

Data availability

Data will be made available on request.

References

[1] A.W.G. Platt, Coord. Chem. Rev. 340 (2017) 62–78.
[2] P.E. Sues, A.J. Lough, R.H. Morris, Inorg Chem. 51 (2012) 9322–9332.
[3] A.M.J. Lees, A.W.G. Platt, Polyhedron 24 (2005) 427–433.
[4] M. Nagomi, M. Hashimoto, Y. Sasoika, R. Tanabe, H. Satou, Energy Procedia 71 (2015) 427–433.
[5] K. Miyata, Y. Hasegawa, Y. Kuramochi, T. Nakagawa, T. Yokoo, T. Kawai, Eur. J. Inorg. Chem. (2009) 4777–4785.
[6] T. Tanase, K. Nakamae, Y. Okawa, M. Hamada, A. Matsumoto, T. Najajima, T. Kawai, Chem. Eur. J. 28 (2022) e202104060.
[7] V.K. Brel, Y.V. Fedorov, A.V. Vologzhanina, P.V. Dorovatovskii, Inorg. Chem. Comm. 146 (2022) 110181.
[8] H.C. Aspinall, J.S. Bissett, N. Greeves, D. Levin, Tet. Lett. 43 (2002) 323–325.
[9] S. Kobayashi, M. Sugiura, H. Kitagawa, W.-W.-L. Lam, Chem. Rev. 102 (2002) 2227–2302.
[10] D.A. Evans, J. Wu, J. Am. Chem. Soc. 125 (2003) 10162–10163.
[11] F.Zhou, J.Wu, M.Lin, Y.Zhao, J.Wu, Y.Zhang, W.Li, Y.Li, Z. Anorg. Allg, Chem. 637 (2011) 117-121.
[12] H.C. Aspinall, J.L. Dwyer, J.L.M. Greeves, N. McIver, J.C. Wooley, Organometallics 17 (1998) 1884–1888.
[13] S.J. Coles, L.J. McCormick McPherson, A.W.G. Platt, K. Singh, Molecules 29 (2024) 2580.
[14] S. Alvarez, P. Alemany, D. Casanova, J. Cirera, M. Llunell, D. Avnir, Coord. Chem. Rev. 249 (2005) 1693–1708.
[15] M.Llunell, D.Casanova, J.Cirera, P.Alemany, S.Alvarez, SHAPE – Program for the Stereochemical Analysis of Molecular Fragments by Means of Continuous Shape Measures and Associated Tools, Version 2.1, University of Barcelona, Spain, 2013Shape.
[16] M. Mantina, A.C. Chamberlin, R. Valero, C.J. Cramer, D.G. Truhlar, J. Phys. Chem. A 113 (2009) 5806–5812.
[17] J. Fawcett, A.W.G. Platt, Polyhedron 22 (2003) 967–973.
[18] A. Bowden, A.W.G. Platt, K. Singh, R. Townsend, Inorg. Chim. Acta. 363 (2002) 243–249.
[19] T. Luster, H.J. Van de Roovaart, K.J. Korman, G.G. Sands, K.M. Dunn, A. Spyker, R. J. Staples, S.M. Biros, J.E. Bender, Dalton Trans. 51 (2022) 9103–9115.
[20] D.H. Johnson, D.F. Shriver, Inorg. Chem. 32 (1993) 1045–1047.
[21] G.A. Lawrance, Chem. Rev. 86 (1986) 17–33.
[22] S.O. Grim, R.C. Barth, J.D. Mitchell, J. Del Gadio, Inorg. Chem. 16 (1977) 1776–1779.
[23] L.L. Bean, D. Phillips, L. Polensek, Can. J. Chem. 59 (1981) 50–61.
[24] T. Tsuchimoto, T. Maeda, E. Shirakawa, Y. Kawakami, Chem. Commun. (2000) 1573–1574.
[25] J. Fawcett, A.W.G. Platt, D.R. Russell, Polyhedron 21 (2002) 287–293.
[26] B. DiMarco, G.G. Bombi, Mass Spectrom. Rev. 25 (2006) 347–379.
[27] G.M. Sheldrick, ShelXT-Integrated space-group and crystal-structure determination, *Acta Cryst* A 71 (2015) 3–8.
[28] O.V. Dolomanov, L.J. Bourhis, R.J. Gildea, J.A.K. Howard, H. Puschmann, Olex2: A complete structure solution, refinement and analysis program, *J. Appl. Cryst.* 42 (2009) 339–341.
[29] G.M. Sheldrick, Crystal structure refinement with ShelXL, *Acta Cryst* C 27 (2015) 3–8.
[30] CrysAlisPro Software System, Rigaku Oxford Diffraction, (2019).
[31] DENZO - Data collection and processing software: Z. Otwinowski, W. Minor in *Methods in Enzymology*, *Vol 276*; *Macromolecular Crystallography*, *part A*, (Eds.: C. W. Carter, Jr, R. M. Sweet), Academic Press, London, 1997, pp. 307-326.
[32] COLLECT - Data collection software, R. Hooft, Nonius B.V. (1998).
[33] Unit cell determination using DirAx: a) A. J. M. Duisenberg, *J. Appl. Crystallogr.* 25 (1992) 92-96; b) A. J. M. Duisenberg, R. W. W. Hooft, A. M. M. Schreurs, J. Kroon, *J. Appl. Crystallogr.* 33 (2000) 893-898.
[34] Absorption correction: G. M. Sheldrick, SADABS. Version 2007/2. Bruker AXS Inc., Madison, Wisconsin, USA.
[35] SHELX-2013: G. M. Sheldrick, *Acta Cryst.* A64 (2008) 112-122.
[36] WinGX: L. J. Farrugia, *J. Appl. Crystallogr.* 45 (2012) 849-854.
[37] Mercury 4.3.1, CCDC: C. F. Macrae, I. Sovago, S. J. Cottrell, P. T. A. Galek, P. McCabe, E. Pidcock, M. Platings, G. P. Shields, J. S. Stevens, M. Towler, P. A. Wood, J. Appl. Cryst. 53 (2020) 226-235.
[38] S.J. Coles, P.A. Gale, Chem. Sci. 3 (2012) 683–689.